Available online at www.sciencedirect.com

SciVerse ScienceDirect

Ceramics International 39 (2013) 911–916

CERAMICS INTERNATIONAL

www.elsevier.com/locate/ceramint

Synthesis and characterization of boron doped bismuth–calcium–cobalt oxide nanoceramic powders via polymeric precursor technique

Arda Aytimur[a], İbrahim Uslu[a,*], Emre Çınar[b], Serhat Koçyiğit[a], Fatih Özcan[c], Ahmet Akdemir[b]

[a]*Gazi Faculty of Education, Gazi University, Teknikokullar, Ankara, 06500, Turkey*
[b]*Faculty of Engineering and Architecture, Selçuk University, Selçuklu, Konya 42090, Turkey*
[c]*Faculty of Science, Selçuk University, Selçuklu, Konya 42090, Turkey*

Received 20 April 2012; received in revised form 21 June 2012; accepted 1 July 2012
Available online 10 July 2012

Abstract

In this study, boron doped calcium stabilized bismuth cobalt oxide nanocrystalline ceramic powders were successfully prepared from aqueous boric acid containing calcium–bismuth–cobalt acetate/poly(vinyl alcohol) hybrid precursor polymer solutions. Then, obtained ceramic powders were characterized via FT-IR, XRD, and SEM techniques. According to X-ray results, fcc and bcc phases coexist in the samples of the nanocrystalline ceramic powders. fcc peaks became sharper and bcc peak decreased with increasing boron content. Structural parameters for face centered cubic structure were calculated using the Scherrer equation. Moreover, dislocation densities and microstrain values were calculated for the nanocrystalline powder samples.

Keywords: A. Sol–gel processes; A. Calcination; B. Nanocomposites; B. Grain size

1. Introduction

Calcium–cobalt oxide composite materials through the control of carrier density and mobility were reported to have high thermoelectric properties [1–7]. The substitution of some amount of Bi for Ca causes an increase in both the electrical conductivity and the thermoelectric power simultaneously [7]. Both the electrical conductivity and the Seebeck coefficients increased in line with the increase of the Bi content in the composite material, which is attributed to the increase of carrier mobility due to the larger size (0.117 nm) of Bi ions [5]. Bi_2O_3 exhibits a number of polymorphs [8,9], but cubic δ-Bi_2O_3 phase attracts particular attention. Unfortunately, the δ-Bi_2O_3 is only stable in a temperature range varying between 730 and 825 °C. When cooler, the δ-Bi_2O_3 phase transforms to metastable forms and the conductivity drops over three orders of magnitude [10,11]. When hotter, the δ-Bi_2O_3 phase can be retained at lower temperatures by doping Bi_2O_3 with the rare earth or alkali earth's oxides such as Ca oxides. Therefore, using Ca gives us the opportunity to kill two birds with one stone, by ensuring cubic δ-Bi_2O_3 phase stability, and providing an increase in the Seebeck coefficient and optimizing the electrical conductivity.

In this study, δ-phase boron doped bismuth–calcium–cobalt oxide nanocrystalline powders are synthesized by calcination and the organic phase of the precursor hybrid polymer solution containing boric acid and Bi/Ca/Co acetate/poly(vinyl alcohol) (PVA) is removed.

The addition of boron oxide to the composite materials is very beneficial. It reduced the processing temperature with its low melting point and as such could help during the calcination stage, resulting in smaller grain sizes and strengthening the grain boundary. Smaller grains have greater ratios of surface area to volume, which means a greater ratio of grain boundary to dislocations. The more grain boundaries

*Corresponding author. Tel.: +90 312 202 8017; fax: +90 312 202 8041.
E-mail address: uslui_1955@yahoo.com (İ. Uslu).

0272-8842/$36.00
http://dx.doi.org/10.1016/j.ceramint.2012.07.005

that exist, the higher the strength becomes. Thus, an easy way to improve the strength of a material is to make the grains as small as possible, increasing the amount of grain boundary. In this study, boric acid was chosen as the cheapest and nontoxic source of boric oxide [12–15].

2. Experimental section

2.1. Materials and method

In the experiments, PVA (Mw 85,000–124,000 g/mol), bismuth(III) acetate and calcium acetate were obtained from Sigma Aldrich, cobalt(II) acetate and boric acid were obtained from Merck, and ultrapure deionized water was used as a solvent.

Multicomponent oxide ceramic powders can be produced via solid state reaction technique. The conventional synthesis of multicomponent composite powders consists of repeated cycles of milling and calcination processes carried out to achieve the solid-state reaction of multicomponent oxide ceramic powders. The difficulty of repeated mixing and milling of the powders and poor chemical homogeneity are main disadvantages of this technique.

The polymer precursor technique has been proven to be one of the suitable methods for the preparation of multicomponent composite oxide in low temperature under 850 °C [16]. The main advantages of polymeric precursor techniques are the homogeneity of the precursors on a molecular level and the low processing temperatures [17–20].

2.2. Sol preparation

An aqueous PVA solution (10%) was first prepared by dissolving the PVA powder in distilled water and heating it at 80 °C while stirring for 3 h, then cooling it down to room temperature. In the experiments, three hybrid polymer solutions were prepared. For each composition, proper proportions of metal acetate solutions were added drop by drop to the 20 g aqueous PVA (10% w/w) at 60 °C (see Table 1 for details) and each hybrid polymer solutions were stirred vigorously using a magnetic stirring bar for 3 h at this temperature. As a final product, viscous gels of both boron doped and undoped PVA/Bi–Ca–Co acetate hybrid polymer solutions were prepared. The prepared solutions and values of solution components are given in Table 1. The hybrid polymer solutions were dried at room temperature and finally were transferred into a ceramic crucible, and then, calcined in air atmosphere at 850 °C for 2 h at a heating and cooling rate of 8 °C/min. The resulting oxide ceramic composites obtained from solutions 1–3, named as PPT 1–3, were ground into powder using a mortar.

2.3. Measurement and characterization

The pH and conductivity of the solutions were measured by using a Wissenschaftlich-Technische-Werkstätten WTW and 315i/SET apparatus. The viscosity of the hybrid polymer solutions was measured with AND SV-10 viscometer. The surface tension of the complex hybrid polymer solutions was measured by using the KRUSS model manual measuring system. Fourier Transformations Infrared Spectroscopy (FT-IR) with ATR module results was obtained using a Thermo Nicolette 6700 spectrophotometer. The crystal structures of the calcined powders were investigated by means of X-ray diffraction (XRD) (Bruker AXS D8 Advance diffractometer with Vario1 Johansson focusing monochromator Cu Kα1 radiation).

3. Results and discussion

The pH, the viscosity, the conductivity and the surface tension of the PVA/Bi–Ca–Co acetate solution were measured and are given in Table 2. The addition of boric acid as the boron source increased the viscosity, the surface tension

Table 1
Value of the polymer solution components.

Solution #	Value of Components (g)				
	Bismuth acetate	Calcium acetate	Cobalt acetate	Boric acid	PVA solution
PPT-1	2	1.3688	1.2902	–	20
PPT-2	2	1.3688	1.2902	0.0160	20
PPT-3	2	1.3688	1.2902	0.0800	20

Table 2
Physical properties of the polymer solutions.

Solution #	pH	Conductivity (mS cm)	Viscosity (mPa s)	Surface Tension (mN/m)
PPT-1	3.49	10.11	20.4	46
PPT-2	3.55	10.03	28.2	47
PPT-3	3.69	10.93	52.7	49

and the pH of the hybrid polymer solution as expected, since boron was used as a cross-linking agent in this study.

FTIR spectroscopy was performed to gain information about the structures of calcined powders. Fig. 1 is the FT-IR spectra of the nanocrystalline powder samples. The bands, which were observed at 1407, 871, 711 and 665 cm^{-1}, are thought to arise due to the bismuth oxide, cobalt oxide or calcia. The bands observed at 1276 cm^{-1} and 1224 cm^{-1} are attributed to the asymmetric stretching vibrations of B–O bonds from ortho–borate groups [21].

XRD data of the nanocrystalline composite samples given in Fig. 2 show that a partial decomposition of fcc phase to bcc phase takes place for all samples, however, fcc peaks became sharper and bcc (110) peak decreased with increasing boron content. Boron doping resulted into a progressive increase of the fcc crystallite size indicating

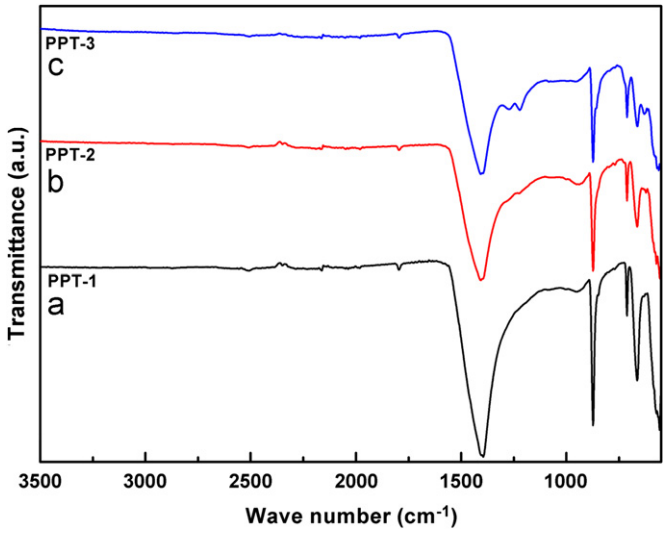

Fig. 1. FT-IR spectra of nanocrystalline: (a) PPT-1, (b) PPT-2, and (c) PPT-3 ceramic powder samples.

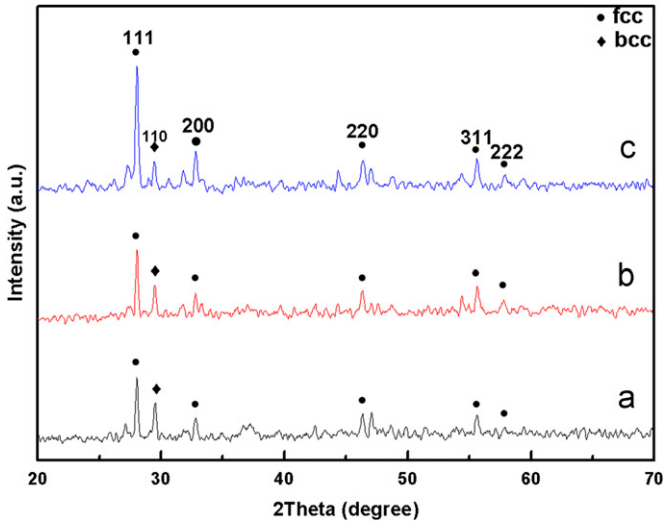

Fig. 2. X-ray diffraction patterns of the crystalline structure of sintered boron doped and undoped Bi–Ca–Co nanocrystalline composite powders obtained from solutions: (a) PPT-1, (b) PPT-2, and (c) PPT-3.

that the crystallinity and stability of the Bi_2O_3–CaO–CoO_2 system is accelerated by the increase of the boron content. This trend is in accordance with the SEM results given below. The crystal structure directly affects the mechanical and electrical properties of the composite material. As an example, the hardness and strength increase with the increasing amount of bcc phases, but the composite ceramic material gets brittle. It is certainly important to be able to control the formation of the bcc phases in the composite material [22–25].

The crystallite size (D) was calculated based upon the main diffraction peaks' broadening in the XRD pattern using the Scherrer formula [26–30].

$$D_{hkl} = \frac{k\lambda}{\beta_{hkl}\cos\theta} \quad (1)$$

where D_{hkl} is the average dimension of the crystallites, $k = 0.9$, λ is the wavelength of the X-ray radiation (0.15405 nm), θ is the Bragg angle for the crystal planes $\{hkl\}$, and β_{hkl} is the broadening (full-width at half-maximum (FWHM)) of the peak.

The lattice parameters of the composite samples were determined by comparing the peak positions (2θ) of the XRD patterns using the below relations [31]:

$$\frac{1}{d^2} = \frac{h^2+k^2+l^2}{a^2} \quad (2)$$

The calculated structural parameters of the composite samples for the fcc phase are given in Table 3. According to the calculation results, average structural lattice parameters of the fcc phase, a, were given as 5.486 nm, 5.484 nm, and 5.484 nm for the PPT-1, PPT-2, PPT-3 samples, respectively. Crystallite size (D) was calculated, for the main reflection (111) peak using Eq. (1), as 46.48 nm (4.648×10^{-8} m), 50.49 nm (5.049×10^{-8} m), and 44.22 nm (4.422×10^{-8} m) for the PPT-1, PPT-2, and PPT-3, respectively. As given in Table 4, the fcc and bcc phases coexist in the samples and their calculated structural parameters were given in the same table for comparison purposes. As expected the bcc structural

Table 3
Calculated structural parameters of the composite samples for fcc phase.

Sample	(*hkl*)	2*θ* (deg.)	FWHM (deg.)	*d* (Å)	*a* (Å)
PPT-1	(111)	28.10	0.1767	3.1729	5.4956
	(200)	32.83	0.2725	2.7258	5.4515
	(220)	46.43	0.2863	1.9541	5.5271
	(311)	55.69	0.3043	1.6491	5.4696
PPT-2	(111)	28.10	0.1622	3.1729	5.4956
	(200)	32.83	0.2446	2.7258	5.4515
	(220)	46.50	0.3137	1.9513	5.5192
	(311)	55.70	0.3000	1.6489	5.4686
PPT-3	(111)	28.10	0.1852	3.1729	5.4956
	(200)	32.83	0.2426	2.7258	5.4515
	(220)	46.49	0.3806	1.9517	5.5203
	(311)	55.69	0.2256	1.6491	5.4696

lattice parameters are lower than the fcc phase and all the results of the samples are in agreement with the JCPDS files 040-0317 and 040-0314 for the fcc and bcc phases, respectively.

Given that the radius of B^{3+} (0.023 nm) is much smaller than that of Bi^{3+} (0.117 nm), it is difficult for B^{3+} to replace the Bi^{3+} site. Thus it is estimated that most boron ions are doped in the interstitial of Bi_2O_3 matrix. Boron

Table 4
Calculated structural parameters of the bcc and fcc structures of the samples.

Sample	Crystal lattice	(*hkl*)	*2θ* (deg.)	FWHM (deg.)	*d* (Å)	*a* (Å)
PPT-1	bcc	(110)	29.50	0.1806	3.0254	4.2786
	fcc	(111)	28.10	0.1767	3.1729	5.4956
PPT-2	bcc	(110)	29.52	0.1691	3.0234	4.2758
	fcc	(111)	28.10	0.1622	3.1729	5.4956
PPT-3	bcc	(110)	29.52	0.1434	3.0234	4.2757
	fcc	(111)	28.10	0.1852	3.1729	5.4956

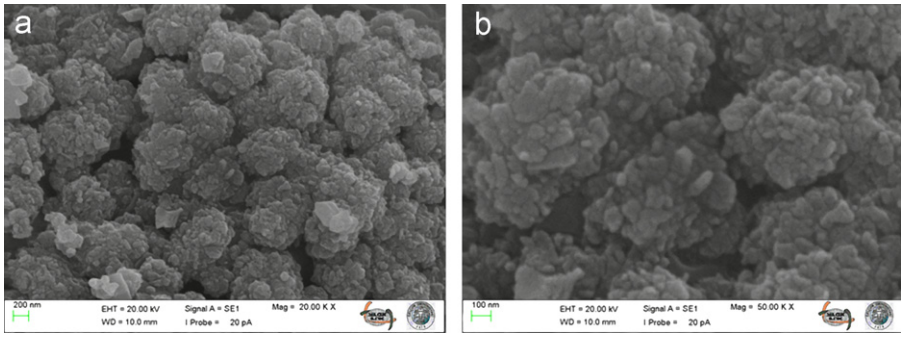

Fig. 3. SEM micrographs of PPT-1 sample. SEM analysis shows that more severe agglomeration occurred in PPT-1 samples.

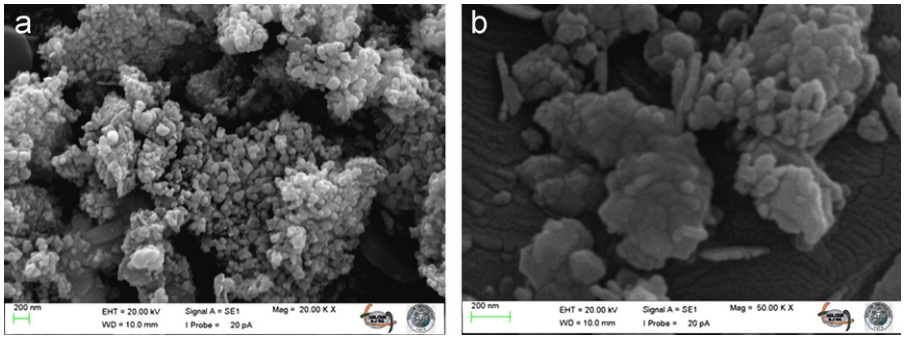

Fig. 4. SEM micrographs of PPT-2 sample. The figure shows that boron doping decreased the diameter of agglomerates.

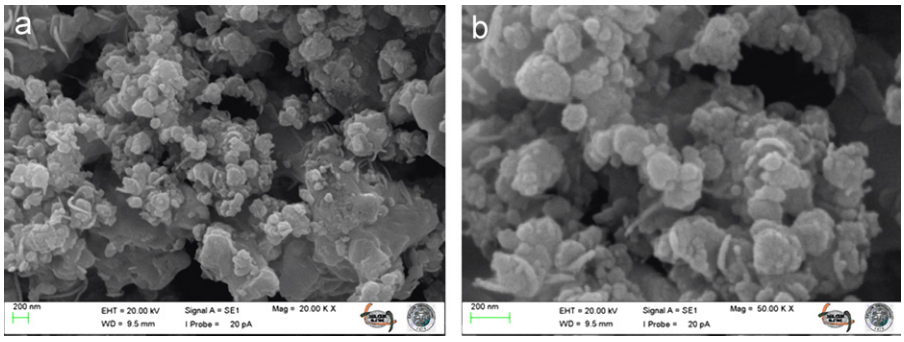

Fig. 5. SEM micrographs of PPT-3 sample. SEM micrographs show that the grain size tend to become small and uniform when the boron doping decreased the agglomeration and grain sizes considerably.

ions may enter the interstitial site of Bi_2O_3 crystal structure and lead to the swell of the crystallite size. Further increase of the boron may cause a decrease in crystallite size and transition to the amorphous glassy structure which is consistent with literature [32].

In addition, the crystallite size (D) is related to the dislocation density (δ) of the undoped calcia stabilized bismuth oxide nanoceramic powder as given by

$$\delta = \frac{n}{D^2} \tag{3}$$

where n is a factor ($n=1$ for minimum dislocation density) [31]. The microstrain values (ε) in the Bi_2O_3–CaO–CoO_2 nanocrystalline powders can be calculated by using the following relation [26]:

$$\varepsilon = \frac{1}{\tan\theta}\left[\frac{\lambda}{D\cos\theta} - B\right] \tag{4}$$

The calculated microstrain values are 1.369×10^{-3}, 1.257×10^{-3}, and 1.435×10^{-3} for the PPT-1, PPT-2, and PPT-3 samples, respectively. The calculated dislocation density values are $4.656\times10^{10}\,cm^{-2}$, $3.923\times10^{10}\,cm^{-2}$, and $5.115\times10^{10}\,cm^{-2}$ for the PPT-1, PPT-2, and PPT-3 samples, respectively.

The morphology and structure of the nanostructured powders obtained were determined by the SEM given in Figs. 3–5. Observations in Fig. 3(a, b) show that boron undoped (PPT-1) structure consists of large agglomerates (ranging from 621 to 843 nm in diameter with an average of 727 nm) composed of spherical grains. Boron addition to the PPT-2 sample decreased the diameter of the agglomerates as shown in Fig. 3(a, b). According to SEM micrographs, the best crystalline structure was obtained for the PPT-3 sample (see Fig. 4). We have obtained homogeneous nanograin structure (nanograins ranging from 51 to 83 nm in diameter with an average of 65 nm) when we increased the boron doping. The XRD analysis and the XRD results calculated from Debye Scherrer's formula also confirms these results given above.

4. Conclusions

Boron doped Bi_2O_3–CaO–CoO_2 nanocrystalline powders were produced via polymeric precursor method. Obtained nanocrystalline powders were characterized by FT-IR, XRD, and SEM techniques. The XRD data of the nanocrystalline composite samples show that a partial decomposition of the fcc phase to the bcc phase takes place for all samples, however, the fcc peaks became sharper and the bcc (110) peak decreased with increasing boron content. Composites doped with B_2O_3 exhibited smaller grain sizes and therefore had higher flexural strengths as compared to composites without B_2O_3. Crystallite size (D) was calculated as 46.48 nm (4.648×10^{-8} m), 50.49 nm (5.049×10^{-8} m), and 44.22 nm (4.422×10^{-8} m) for the undoped, 0.8% boron doped and 4% boron doped samples, respectively. SEM results show that boron undoped structure consists of large agglomerates composed of spherical grains, and boron addition to the samples decreased the diameter of the agglomerates.

References

[1] Y.F. Zhang, J.X. Zhang, Q.M. Lu, Rapid synthesis of $Ca_2Co_2O_5$ textured ceramics by coprecipitation method and spark plasma sintering, Journal of Alloys and Compounds 399 (2005) 64–68.

[2] Y.F. Zhang, J.X. Zhang, Rapid reactive synthesis and sintering of textured $Ca_3Co_4O_9$ ceramics by spark plasma sintering, Journal of Materials Processing Technology 208 (2008) 70–74.

[3] S. Li, R. Funahashi, I. Matsubara, K. Ueno, S. Sodeoka, H. Yamada, Synthesis and thermoelectric properties of the new oxide materials $Ca_{3-x}Bi_xCo_4O_{9+\delta}$ ($0.0<x<0.75$), Chemistry of Materials 12 (2000) 2424–2427.

[4] S. Li, R. Funahashi, I. Matsubara, H. Yamada, K. Ueno, S. Sodeoka, Synthesis and thermoelectric properties of the new oxide ceramics $Ca_{3-x}Sr_xCo_4O_{9+\delta}$ ($x=0.0$–1.0), Ceramics International 27 (2001) 321–324.

[5] Y. Masuda, D. Nagahama, H. Itahara, T. Tani, W.S. Seo, K. Koumoto, Thermoelectric performance of Bi- and Na-substituted $Ca_3Co_4O_9$ improved through ceramic texturing, Journal of Materials Chemistry 13 (2003) 1094–1099.

[6] Y.F. Zhang, J.X. Zhang, Q.M. Lu, Synthesis of highly textured $Ca_3Co_4O_9$ ceramics by spark plasma sintering, Ceramics International 33 (2007) 1305–1308.

[7] G. Xu, R. Funahashi, M. Shikano, I. Matsubara, Y. Zhou, Thermoelectric properties of the Bi- and Na-substituted $Ca_3Co_4O_9$ system, Applied Physics Letters 80 (2002) 3760–3762.

[8] H. Jeen, G. Singh-Bhalla, P.R. Mickel, K. Voigt, C. Morien, S. Tongay, A.F. Hebard, A. Biswas, Growth and characterization of multiferroic $BiMnO_3$ thin films, Journal of Applied Physics 109 (7) (2010), http://dx.doi.org/10.1063/1.3561860.

[9] C. Guo, S.Z. Pu, Z.L. Chen, M.Y. Li, J.F. Cao, H.M. Zou, TEM study of a fluorite-type $(1-x)Bi_2O_3\cdot xFe_2O_3$ superstructure in $BiFeO_3$ ceramics synthesized by the rapid liquid-phase sintering method, Ceramics International 36 (2010) 507–512.

[10] J.A. Switzer, M.G. Shumsky, E.W. Bohannan, Electrodeposited ceramic single crystals, Science 284 (1999) 293–296.

[11] H.T. Fan, S.S. Pan, X.M. Teng, C. Ye, G.H. Li, L.D. Zhang, δ-Bi_2O_3 thin films prepared by reactive sputtering: fabrication and characterization, Thin Solid Films 513 (2006) 142–147.

[12] M Takeyama, C.T. Liu, Effects of grain size and test temperature on ductility and fracture behavior of a B-doped Ni_3Al alloy, Acta Metallurgica Sinica 36 (1988) 1241–1249.

[13] Z.W. Zhang, C.T. Liu, S. Guo, J.L. Cheng, G. Chen, T. Fujita, M.W. Chen, Y.W. Chung, S. Vaynman, M.E. Fine, B.A. Chin, Boron effects on the ductility of a nano-cluster-strengthened ferritic steel, Materials Science and Engineering A-Structural Materials Properties Microstructure and Processing 528 (2011) 855–859.

[14] J.M. Ting, Sintering of silicon carbide/molybdenum disilicide composites using boron oxide as an additive, Journal of the American Ceramic Society 77 (1994) 2751–2752.

[15] S. Durmusoglu, I. Uslu, T. Tunc, S. Keskin, A. Aytimur, A. Akdemir, Synthesis and characterization of boron-doped Bi_2O_3–La_2O_3 fiber derived nanocomposite precursor, Journal of Polymer Research 18 (2011) 1999–2004.

[16] T. Suzuki, I. Kosacki, H.U. Anderson, Defect and mixed conductivity in nanocrystalline doped cerium oxide, Journal of the American Ceramic Society 85 (2002) 1492–1498.

[17] H. Liu, Y. Luo, M. Li, Preparation of submicron LaCaMnO submicron powder and LaCaMnO–alumina composites with CMR effects by a new method: precursor sintering technique, Journal of Materials Processing Technology 202 (2008) 347–352.

[18] R. Riedel, G. Mera, R. Hauser, A. Klonczynski, Silicon-based polymer-derived ceramics: synthesis properties and applications—a review:

dedicated to Prof. Dr. Fritz aldinger on the occasion of his 65th birthday, Journal of the Ceramic Society of Japan 114 (6) (2006) 425–444.
[19] M.A. Schiavon, K.J. Ciuffi, I.V.P. Yoshida, Glasses in the Si–O–C–N system produced by pyrolysis of polycyclic silazane/siloxane networks, Journal of Non-Crystalline Solids 353 (2007) 2280–2288.
[20] M.A. Schiavon, I.V.P. Yoshida, Ceramic matrix composites derived from $CrSi_2$-filled silicone polycyclic network, Journal of Materials Science 39 (2004) 4507–4514.
[21] A.O. Hulpus, R. Ciceo Lucacel, I. Ardelean, Spectroscopic (FT-IR and Raman) studies on $CuO–B_2O_3–PbO–Ag_2O$ glass systems, Journal of Optoelectronics and Advanced Materials 10 (2008) 3209–3211.
[22] S. Guo, C. Ng, J. Lu, C.T. Liu, Effect of valence electron concentration on stability of fcc or bcc phase in high entropy alloys, Journal of Applied Physics 109 (2011) 103505, http://dx.doi.org/10.1063/1.3587228.
[23] C.J. Tong, Y.L. Chen, S.K. Chen, J.W. Yeh, T.T. Shun, C.H. Tsau, S.J. Lin, S.Y. Chang, Microstructure characterization of Al_xCoCr–CuFeNi high-entropy alloy system with multiprincipal elements, Metallurgical and Materials Transactions A-Physical Metallurgy and Materials Science 36 (2005) 881–893.
[24] C.W. Tsai, M.H. Tsai, J.W. Yeh, C.C. Yang, Effect of temperature on mechanical properties of $Al_{0.5}$CoCrCuFeNi wrought alloy, Journal of Alloys and Compounds 490 (2010) 160–165.
[25] F.J. Wang, Y. Zhang, G.L. Chen, Atomic packing efficiency and phase transition in a high entropy alloy, Journal of Alloys and Compounds 478 (2009) 321–324.
[26] B. Karunagaran, R.T.R. Kumar, D. Mangalaraj, S.K. Narayandass, G.M. Rao, Influence of thermal annealing on the composition and structural parameters of DC magnetron sputtered titanium dioxide thin films, Crystal Research and Technology 37 (12) (2002) 1285–1292.
[27] P.H. Klug, L.E. Alexander, X-ray Diffraction Procedures for Polycrystalline and Amorphous Materials, Wiley, New York, 1974.
[28] N.S. Prasad, K.B.R. Varma, Nanocrystallization of $SrBi_2Nb_2O_9$ from glasses in the system $Li_2B_4O_7–SrO–Bi_2O_3–Nb_2O_5$, Material Science and Engineering B-Solid State Materials For Advanced Technology 90 (2002) 246–253.
[29] E. Alvarado, L.M. Torres-Martinez, A.F. Fuentes, P. Quintana, Preparation and characterization of MgO powders obtained from different magnesium salts and the mineral dolomite, Polyhedron 19 (2000) 2345–2351.
[30] Y. Ding, G.T. Zhang, H. Wu, B. Hai, L.B. Wang, Y.T. Qian, Nanoscale magnesium hydroxide and magnesium oxide powders: control over size, shape, and structure via hydrothermal synthesis, Chemistry of Materials 13 (2001) 435–440.
[31] C. Suryanarayana, M.G. Norton, X-Ray Diffraction a Practical Approach, Plenum Press, New York, 1998.
[32] D. Chen, D. Yang, Q. Wang, Z.Y. Jiang, Effects of boron doping on photocatalytic activity and microstructure of titanium dioxide nanoparticles, Industrial and Engineering Chemistry Research 45 (2006) 4110–4116.